Available online at www.sciencedirect.com
SCIENCE DIRECT
Tectonophysics 412 (2006) 27–47
TECTONOPHYSICS
www.elsevier.com/locate/tecto

Temperature and density of the Tyrrhenian lithosphere and slab and new interpretation of gravity field in the Tyrrhenian Basin

F. Cella [a], S. de Lorenzo [b], M. Fedi [c], M. Loddo [b], F. Mongelli [b], A. Rapolla [c], G. Zito [b,*]

[a] *Department of Earth Sciences—University of Calabria, Italy*
[b] *Department of Geology and Geophysics—University of Bari, Italy*
[c] *Department of Earth Sciences—University "Federico II" of Naples, Italy*

Received 16 July 2003; accepted 16 August 2005

Abstract

The gravity anomaly field of the Tyrrhenian basin and surrounding regions reflects the complex series of geodynamic events active in this area since the Oligocene–Miocene. They can resume in lithospheric thinning and asthenospheric rising beneath the Tyrrhenian Basin, coexisting with the roll-back subduction of the African plate margin westward sinking beneath the Calabrian Arc. The geographic closeness between these processes implies an intense perturbation of the mantle thermal regime and an interference at regional scale between the related gravity effects.

A model of the litho-asthenospheric structure of this region is suggested, showing a reasonable agreement with both the evidences in terms of regional gravity anomaly pattern and the results concerning thermal state and petro-physical features of the mantle. The first phase of this study consisted of the computation of the isotherms in the crust–mantle system beneath the Tyrrhenian Basin and, afterwards, of the density distribution within the partially melted upwelling asthenosphere. The second phase consisted of a temperature/density modelling of the slab subducting beneath the Calabrian Arc. Finally, a $2^{1/2}$ interpretation of gravity data was carried out by including as constraints the results previously obtained. Thus, the final result depicts a model matching both gravity, thermal and petrographic data. They provide (a) a better definition of the thermal regime of the passive mantle rise beneath the Tyrrhenian basin by means of the estimation of the moderate asthenospheric heating and (b) a model of lithospheric slab subducting with rates that could be smaller than generally suggested in previous works.

Keywords: Tyrrhenian Basin; Central Mediterranean; Subduction; Lithosphere; Asthenosphere; Heat flow; Gravity anomalies; Thermal model; Density model

1. Introduction: the Tyrrhenian Sea–Calabrian Arc system: geophysical setting

The Tyrrhenian basin (Fig. 1) is a deep, asymmetric, depression representing one of the major structural elements of the central Mediterranean. Its Northern part, mostly composed of continental crust, has been interpreted as the western sector of an accretionary prism related to the westwards subduction below Corsica since the early Oligocene (Abbate et al., 1994). Along the western margin the continental basement results thinned by rotational normal faulting (Kastens et al., 1988).

The southern margin of the Tyrrhenian Basin shows a very composite volcanic activity whose products have large petrological differences, from the oldest terms (31–13 My) up to the Aeolian arc (active since 1 My ago) and the Lazio–Campania volcanic districts.

* Corresponding author.
E-mail address: gm.zito@geo.uniba.it (G. Zito).

0040-1951/$ - see front matter © 2005 Elsevier B.V. All rights reserved.
doi:10.1016/j.tecto.2005.08.025

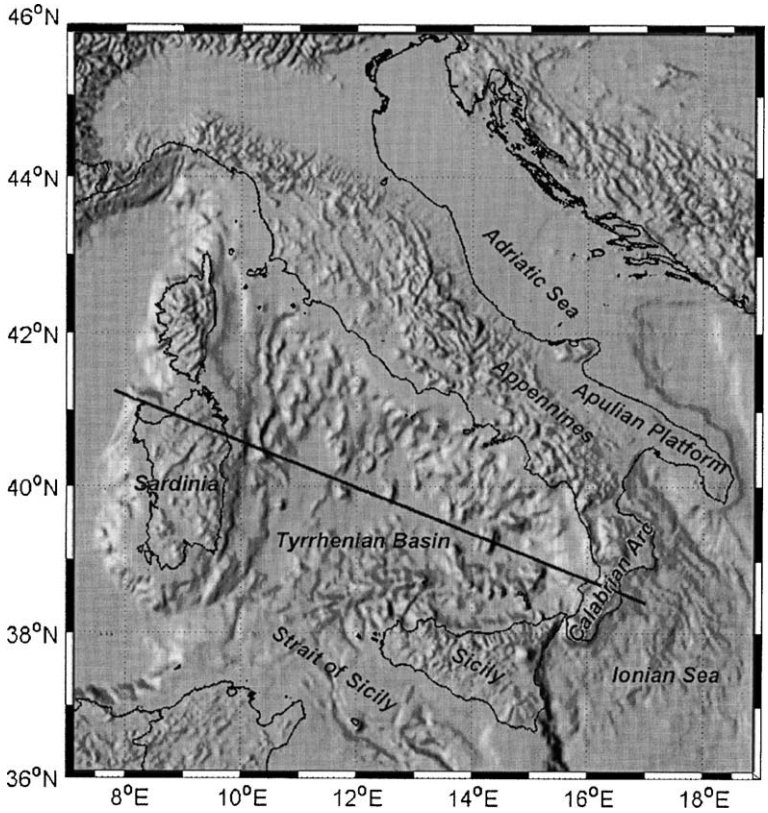

Fig. 1. Regional Sketch map of the main geological and structural features in the Central Mediterranean.

Within the central abyssal plain, a strongly stretched ancient continental crust underwent MORB magmatism (DSDP 373; ODP 650-651-655) and alkali-basaltic volcanic activity (Kastens et al., 1988). The Tyrrhenian Basin is described as an extensional Neogene–Quaternary back-arc basin formed by counterclockwise rotation of the Corsica–Sardinia and Adriatic microplates (Alvarez, 1972; Cherchi and Montadert, 1982; Rehault and Bethoux, 1984). The opening process migrated southeastward and was triggered by the passive westward dipping subduction (Malinverno and Ryan, 1986; Royden et al., 1987; Kastens et al., 1988) of Triassic oceanic lithosphere whose relicts should be present in the Ionian abyssal plain. Such a model agrees with the subduction-related processes like the Apenninic thrust-fold belt (Doglioni, 1991) and the shallower Moho inferred from seismic data (Steinmetz et al., 1983; Recq et al., 1984; Duschenes et al., 1986; Nicolich, 1989; Scarascia et al., 1994), from high heat flow (Della Vedova et al., 1984; Hutchison et al., 1985; Wang et al., 1989; Mongelli et al., 1991; Cataldi et al., 1995, Pasquale et al., 1999) and from the regional gravity field (Morelli, 1970; Corrado and Rapolla, 1981). Further quantitative elements supporting both the strong lithospheric thinning and a passive mantle rise beneath the Tyrrhenian basin came from the density model computed by Cella et al. (1998) not only by merely fitting the regional gravity field but basing also on constraints derived from geothermal information. They were directly inferred from a few available data (i.e. the potential temperature, the β factor and the pre-stretched lithospheric thickness) by means of the petrophysical model provided by McKenzie and Bickle (1988).

The hypothesis of the eastward migration of the rifting process has been recently supported by geophysical investigations (Pasquale et al., 1999; Zito et al., 2003) depicting the present heat flow in the southern Tyrrhenian Sea as a transient thermal wave migrating in time and space. Therefore, the eastward jumping of the spreading centers could be really explained as consequence of the break-up of the earlier Alpine orogen and of the roll-back of the slab that developed eastward (Spadini et al., 1995; Gueguen et al., 1997; Doglioni et al., 1998, 1999). Stretched continental block were dispersed by lithospheric boudinage within areas where the mantle melt rises at very shallow depths and solidifies by

loss of latent heat of fusion (Zito et al., 2003). In the Tyrrhenian case, the opening occurred by two rapid and separate episodes, which moved from west to east generating the Vavilov and Marsili subbasins (Zito et al., 2003).

The southeastward migration of both the Tyrrhenian spreading centre and the Ionian arc since the Neogene, is related to the earlier arrival at the subduction hinge of thicker and less dense continental lithosphere represented by Apulian plate, at first along Central Apennines, whereas, along the Calabrian Arc, thinner and denser oceanic lithosphere still forms the slab at depth (Doglioni, 1991).

The existence of a Benioff zone beneath the Southern Apennine and the Calabrian Arc (Caputo et al., 1970; Patacca et al., 1990; Spakman et al., 1993) was confirmed by the presence of several seismicity clusters up to a depth of 500 km (Gasparini, 1982; Finetti and Del Ben, 1986; Anderson and Jackson, 1987; Giardini and Velonà, 1991; Selvaggi and Chiarabba, 1995).

Clashing opinions still exist about the Tyrrhenian subduction, for example, whether the roll back regressive movement is the cause or the effect of back-arc extension, or its timing, variously aged between 30 and 80 My (Boccaletti et al., 1971; Decourt et al., 1986; Doglioni et al. 1998; Faccenna et al., 2001). Similarly, the rate of subduction underneath the Calabrian Arc is largely debated, ranging from 2 up to 6 cm y^{-1} (Patacca et al., 1990; Pasquale et al., 1999; Faccenna et al., 2001; Doglioni et al., 1999; Valera et al., 2003). The other question that is of concern is if the dipping angle has always been high (65~80°) as a consequence of the global, eastward oriented, asthenospheric flow with respect to the lithosphere (Doglioni, 1991; Pasquale et al., 1999), or of its gradual increase (Faccenna et al., 2001).

In the present research the distribution of densities within the Tyrrhenian shallow mantle resulting from Cella et al. (1998) has been updated. Computations have been now based not only on a single geotherm roughly representative of the thermal state of the whole basin, but on a much more complete data set that allowed Zito et al. (2003) to draw different thermal gradients for each sector of the basin. The density distribution within the subducting slab was finally estimated, taking into account the advection of heat in the sinking slab and the heating both by conduction from the hotter asthenosphere and by compression of the lithospheric slab. The resulting data allow to suggest a regional model depicting the structure of the lithosphere–asthenosphere system in the whole region.

2. Geophysical data

2.1. Description of the gravity anomaly pattern

This study is based on several gravity data sets:

- The Bouguer gravity map of the Tyrrhenian Sea (Morelli, 1970);
- The Bouguer gravity map of the Strait of Sicily and of the Ionian Sea (Morelli et al., 1975);
- The Bouguer Gravity Anomaly Map of the Mediterranean Region, (1 : 1,000,000), issued (1989) by the Intergovernmental Oceanographic Commission (IOC-UNESCO), as an overprint of the International Bathymetric Chart of the Mediterranean (IBCM).

All data sets are based upon the 1967 normal gravity formula and on terrain corrections made by assigning a Bouguer density of 2.67 g/cm^3.

The anomaly field was sampled over a broad area (36–46° N; 7–19° E) to provide a step grid (5') coherent with the regional feature of the study (Fig. 2). The problem due to the integration of the gravity modelling with data from the local geoid, was tackled. Therefore, the indirect effect caused by differences between the reference ellipsoid and the geoid was computed in terms of gravity along the profile. The model provided by the GEOMED Project over the Central Mediterranean area was adopted as reference. The resulting effect shows a maximum amplitude having the same order of the average magnitude of the differences between observed and computed profile. Therefore it should be further reduced by means of low-pass filtering and can be neglected without significant consequences because the gravity data profile has been low pass filtered before the interpretation. The gravity field of the central Mediterranean shows a significant correlation with respect to the main regional morphostructural components in the area. In fact, long wavelength, high amplitude, Bouguer positive anomalies are located within the main marine basins (Jonian basin: +310 mGal; Tyrrhenian basin: +250 mGal; Ligurian–Provençal basin: +210 mGal). An exception is the Adriatic basin that represents foreland continental African domain mostly undeformed and shows a rather flat regional gravity field. Patterns of regional negative Bouguer anomalies are detectable in correspondence of continental areas, e.g. the Alpine and Calabrian orogenic wedges, the Apennine thrust/fold belt system and the Corsica–Sardinia microplate. These correlations, together with the high amplitude

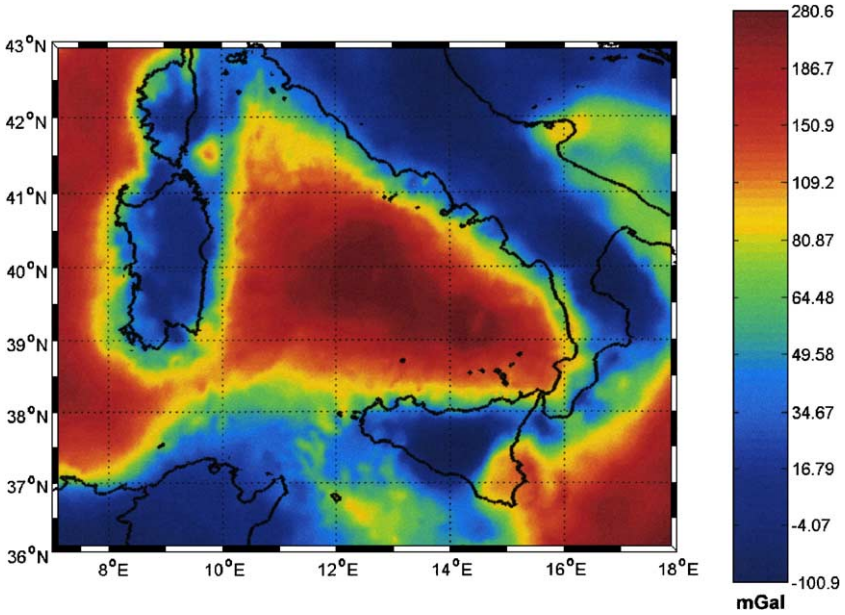

Fig. 2. Bouguer gravity anomaly map of the Central Mediterranean. Reference system IGSN-71; Bouguer density = 2.67 g/cm^3; 1967; normal gravity formula; equidistance = 10 mGal.; step grid (5′); The solid line shows the location of the interpreted gravity profile.

of the anomalies are clearly due to deep sources, i.e. the thickening of the less dense continental lithosphere in the mentioned areas: as often observed in similar cases, the axial gravity placed low on the southern and central Italy is roughly coincident with the external front of the accretionary prism along both the Apennine and Calabrian Arcs.

With regard to the isostatic set-up of the Calabrian Arc, the effect of the crustal roots beneath Calabria was computed by assuming the Airy hypothesis and by assigning a density contrast of 0.5 g/cm^3 between mantle and crust, a maximum topographic height of about 1000 m a.s.l. (in correspondence of the Calabrian Arc) and, finally, an original crust 30 km thick.

The resulting thickness of the compensating root beneath the chain is about 5 km. It implies a high amplitude negative isostatic anomaly and, therefore, a significant tendency to a continental uprising. Several geological evidences and neotectonic studies (Cucci and Cinti, 1999) confirm a quite strong topographic uplift, at least during the quaternary. However, the continental crust is characterized by a compensation depth of about 30 km and by a lateral section less wide than 300 km. This means that the structure would not be wide enough with respect to the compensation depth in order that isostatic adjustments are possible.

In this case, an alternative mechanism to explain the continental uplift has been suggested by Gvirtzman and Nur (1999) that analyzed the topography across subduction zones, considering the separate contributions of the crust and the mantle lithosphere to the continental elevation observed at the surface. They demonstrated that when a slab retreats quickly, as in the Calabrian case, the asthenospheric material flows farther into the plate contact, leading to the loss of suction and plate decoupling. As a result, the heavy slab sinks and the asthenospheric wedge releases overriding the plate from the drag of the slab directly underlying the crust. Consequently the overriding plate rebounds, floating higher than normal. In other words, this means a continental uplift caused neither by classic isostatic adjustment nor by tectonic stress but by other factors related to the dynamic regime of the subduction process.

2.2. Regional heat flow and temperature of the thinned lithosphere and upwelling asthenosphere

Fig. 3 shows the heat flow map of the Tyrrhenian Sea and surrounding areas compiled by Zito et al. (2003). The most conspicuous feature of the map is the high heat flow (rough average 120–130 mW m^{-2}) all over the abyssal plain of the Southern Tyrrhenian Sea. Heat flow decreases towards the continental margins of Corsica–Sardinia block. The lowest values are located offshore Sicily. Two strong local maxima of 143 and 245 mWm^{-2} located over two major sub basin of

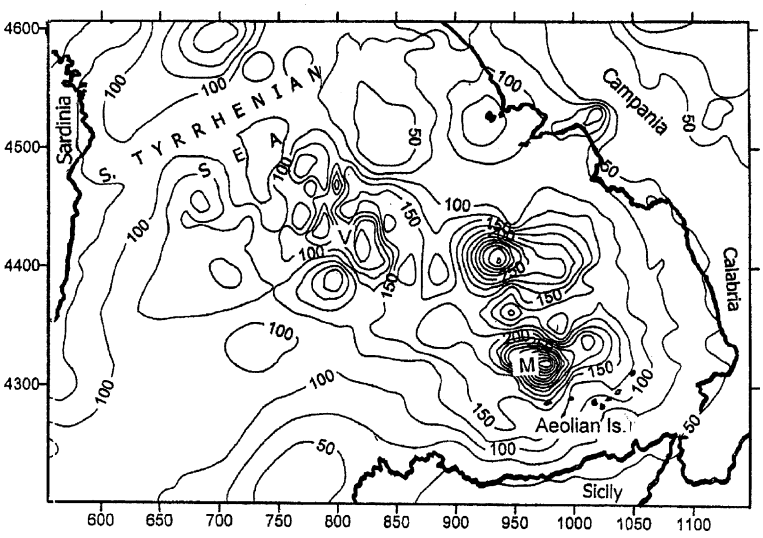

Fig. 3. Heat flow map of the Tyrrhenian Sea and surrounding areas. Contour intervals, 10 mW m^{-2}. After Zito et al., 2003.

the southern Tyrrhenian sea (Fig. 4), i.e. the Vavilov basin and the Marsili basin (Malinverno, 1981; Spadini et al., 1995).Wang et al. (1989) demonstrated that heat flow is not symmetrically distributed about the centre of this young oceanic Tyrrhenian basin. Hutchison et al. (1985) interpreted the regional heat flow value by the simple stretching model of McKenzie (1978). Hutchison et al. (1985) interpreted the observed maximum value at that time of 151 ± 10 mWm^{-2} in the southern Tyrrhenian by the oceanic plate model of Parsons and Sclater (1977). In all these papers the stretching is considered as a unique or continuous event. Recently, new ideas have been elaborated about the stretching of the Tyrrhenian basin (Zito et al., 2003).

As mentioned in the previous section, the rifting of the Tyrrhenian sea started in the Upper Oligocene in the Ligurian–Provencal basin to the west of the Corsica–Sardinia, floored by oceanic crust 19–15 Ma ago (Gueguen et al., 1997). Then the rifting jumped east to the Corsica and Sardinia, proceeding by steps and generating in the southern Tyrrhenian two major basins, i.e. Vavilov basin (7–3.5 Ma) and the Marsili basin (1.7–1.2 Ma). Basalts at the Mt. Vavilov are OIB-MORB type with an age of 4.1 Ma (Sartori, 1989), while the basalts of Mt. Marsili are also calc-alkaline (Beccaluva et al., 1990), and the upper lying sediments have an age of 1.8 Ma (Kastens et al., 1988) indicating a very young basaltic crust.

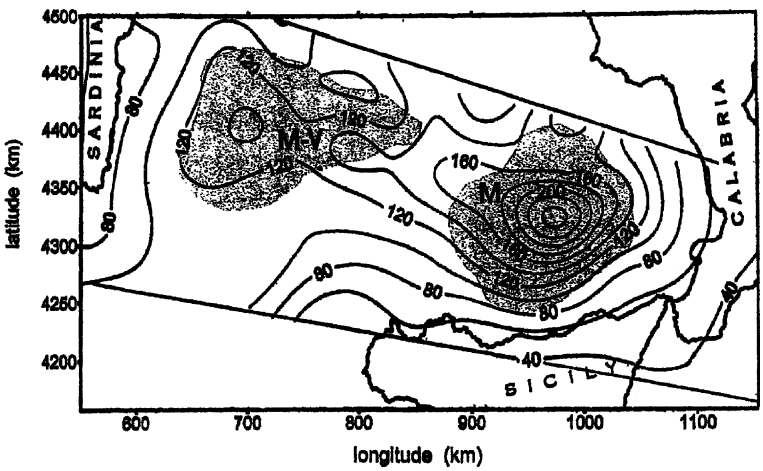

Fig. 4. Smoothed heat flow map of a large strip between Sardinia and Calabrian according to Zito et al. (2003). Contour interval, 20 mW m^{-2}. Dashed areas refers to Magnaghi–Vavilov (M–V) and Marsili (M) basins, respectively.

Zito et al. (2003) modeled these events supposing that in each basin stretching occurred at different times according to the McKenzie model and that further stretching caused the laceration of the thinned lithosphere favoring the passive rising to the surface of an asthenospheric body. They assumed that before the extension the lithosphere had the same structure as the present Alpine Chain: a lithosphere 130 km (Calcagnile and Panza, 1981) and a crust 45–50 km thick (Locardi and Nicolich, 1988 modified by Morelli, 1995). Since the actual thickness of the Tyrrhenian lithosphere is 30 km (Calcagnile and Panza, 1981), in the westernmost sector, and 20 km (Pontevivo and Panza, 2002) in the easternmost sector, Zito et al. (2003) deduced a value $\beta=6.3$ for the older basin and $\beta=7.0$ for the younger one. They calculated the contribution of the rock radioactivity to deep temperatures, as well. Moreover, Zito et al. (2003) studied the cooling of the asthenospheric bodies considering the heat liberated by the solidification (Stefan problem) and deduced the thickness of the new lithosphere.

Fig. 5 shows the geotherms calculated by this model along a profile crossing the southern Tyrrhenian Sea, passing over the Vavilov and Marsili basins.

3. Density distribution in the thinned lithosphere and upwelling asthenosphere

Several studies (Cella and Rapolla, 1997; Cella et al., 1998) pointed out that the thermal state of the upwelling asthenosphere strongly influences the distribution of density within the uprising mantle, causing significant gravity changes. Consequently, a reasonable knowledge of the temperature distribution within the mantle is crucial for a structural modelling by means of gravity data interpretation.

It is well known that the upward migration of the LAB (lithosphere–asthenosphere boundary) can be primarily caused by an active process, i.e. the presence of a "hot plume" having a thermal origin in the lower mantle (Spohn and Shubert, 1982; Courtney and White, 1986). Alternatively, mantle rising and progressive lithospheric thinning are a passive process due to an extensional regime driven, for example, by external forces triggered by the roll-back of sinking slabs (Forsyth and Uyeda, 1975; Angelier and Le Pichon, 1979) and intensified by the convective removal of the lower lithosphere by a delamination process (Schott and Schmeling, 1998) or by sublithospheric dragging and erosion (Mongelli and Zito, 2000).

When the mantle rises and the isotherms upward migrate, the temperature increases reaching the mantle solidus by adiabatic decompression and partial melting occurs. The amount of melt fraction and its composition primarily depend on some factors: (a) the potential temperature (T_p), i.e. the temperature that a fluid mass would have if it were compressed or expanded at a constant reference pressure. With increasing values of T_p the transition from absence (passive upwelling) to presence (active rising) of thermal anomalies occurs; (b) the stretching factor β (McKenzie, 1978), i.e. the ratio of the final to initial surface area involved in the rifting process. With increasing values of β the transition from "continental" to "oceanic" rifting occurs; (c) lithospheric thickness prior to the thinning process starts; increasing values reduce the partial melting process.

On the other hand, also the changes in density within the uprising asthenosphere are controlled by several elements: (a) distribution of temperature within the upwelling mantle, (b) changes in amount of partial melting; (c) changes in melt composition; (d) changes in composition of the mantle rocks after the magma segregation; (e) dependence of density of the liquid and solid fractions on pressure and temperature.

The first step was the computation of new geotherms in the uppermost mantle. Significant improvements resulted with respect to previous works (Cella and Rapolla, 1997; Cella et al., 1998). The second step was the computation, based on the model of McKenzie and Bickle (1988), of the amount of melt fraction and of its chemical composition as function of the geotherms and of the degree of lithospheric stretching. The MORB pyrolite with Fo90 (MPY90) composition (Fallon and Green, 1987) was chosen as representative of a typical upper mantle source.

Very small amounts of liquid fraction remain in the residual mantle rock after melt segregation and migration (McKenzie, 1984); therefore the melt composition allows to infer the chemical composition of the residual mantle. The third step was the computation of the modal norm of the residual mantle rock by treating the problem in terms of solution of component transformations, in which both the global chemical composition of the rock and the composition of any phase component of the rock are known, whereas the amount of any phase component must be determined (Spear et al., 1982; Sebastian, 1989; Cella and Rapolla, 1997). The problem was solved basing on the "minimum length" solution for undetermined linear problems (Menke, 1984; Cella and Rapolla, 1997). Three different input data sets were used depending on the mantle composition depth for which the computation was done (depth > 70 km → garnet peridotite; 30 km < depth < 70

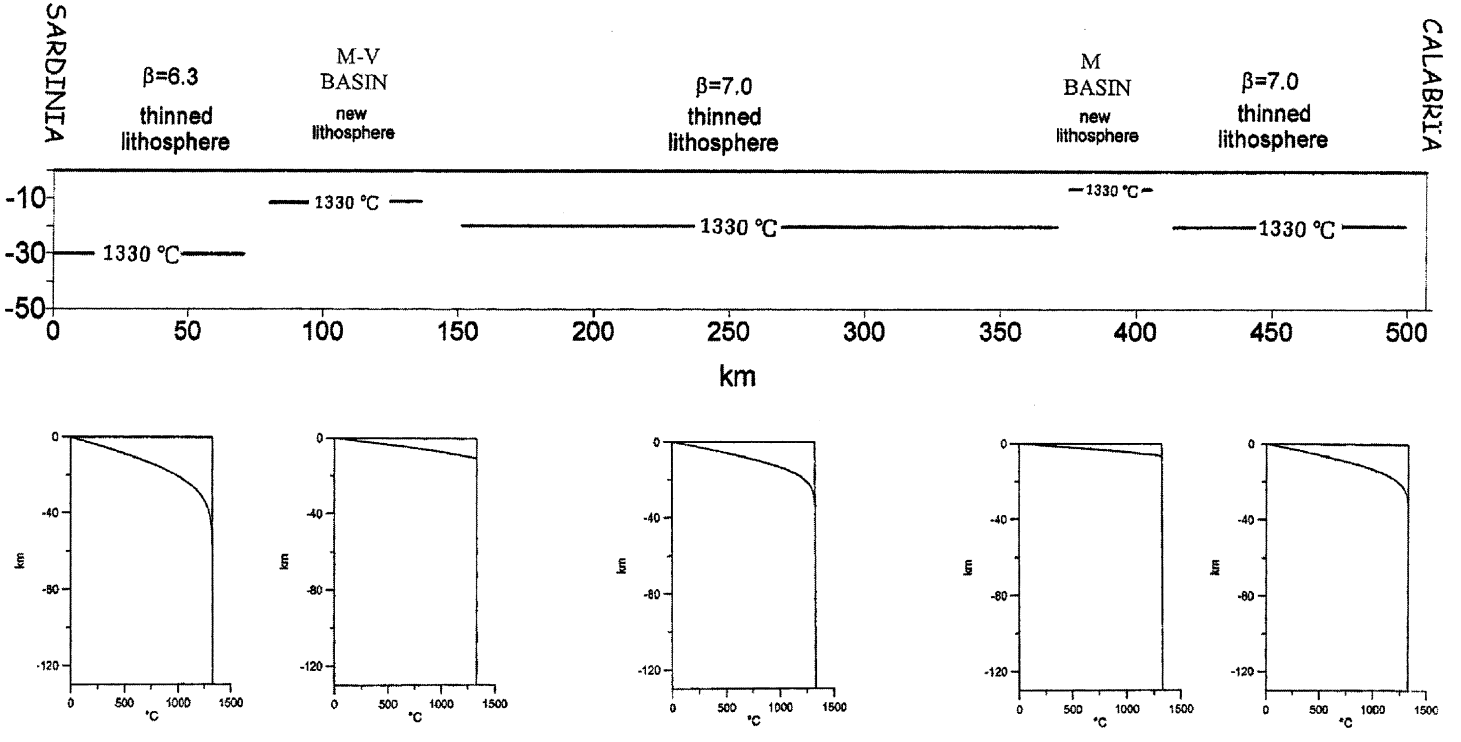

Fig. 5. Lithospheric thickness along the strip of Fig. 4 and geotherms characterizing each sector.

km→spinel peridotite; depth<30 km→plagioclase peridotite) (Green, 1991).

In the last step, the density distribution in the upwelling asthenosphere was finally computed as a function of temperature, pressure and normative composition, by exploiting the model by Niu and Batiza (1991a,b,c). Basing on a quantitative relation between the mantle potential temperature and the vertical displacement of the earth surface (McKenzie and Bickle, 1988; White and McKenzie, 1988), the Tyrrhenian bathial plain, located at a depth of 3000–4000 m, necessarily implies at the LAB a temperature not higher than some tens exceeding the normal. Such a hypothesis was reasonable since previous studies (Keen, 1985) verified that the active mantle upwelling, implying high thermal anomalies, can laterally extend only in areas much larger than the Tyrrhenian Basin. Further confirmations came which have been provided a gravity approach (Cella et al., 1998) and by detailed studies on the heat flux within the Tyrrhenian area (Pasquale et al., 2003; Zito et al., 2003) confirming a potential temperature of 1320–1330 °C. Therefore, the computations were carried out by setting input data for a passive mantle rising model (T_p= 1330 °C). In addition, a value β=6.3–7 was chosen following Zito et al. (2003) that, in agreement with Hutchison et al. (1985) and basing on the heat flow anomalies, predicted a significant degree of thinning (>6), able to cause lithospheric laceration. As far as the pre-rift lithosphere thickness is concerned, a value of 115–130 km was chosen in agreement with previous studies (Pasquale et al., 2003; Zito et al., 2003). In correspondence of the two main positive Tyrrhenian heat flow anomalies, the thermal model predicts an asthenosphere rising nearly up to the base of the stretched crust. Here, material mainly consists of basalt dykes derived from asthenospheric partial fusion and upward melt migration.

The vertical density distribution was computed for each of the geotherms computed along the transect. Melting degree results to upward increase reaching 20–25%. The density gradients computed for most profiles are rather similar for depths ranging from 140 and 50 km. (Fig. 6). For depths lower than 50 km, the density gradients can be grouped in two main vertical profiles. The first one concerns the areas marked by the two positive heat flow anomalies within the abyssal plain and exhibits at shallow depth the lowest density values (Fig. 7a). The second one interests the most part of the basin and a slightly less intense thermal gradient with lower melting degree and denser residual mantle rocks (Fig. 7b).

The computed mantle densities change within rather broad ranges, from 3.35 g/cm^3 (depth ≈ 100 km) to 3.12 g/cm^3 (depth ≈ 10 km) to 3.06 g/cm^3

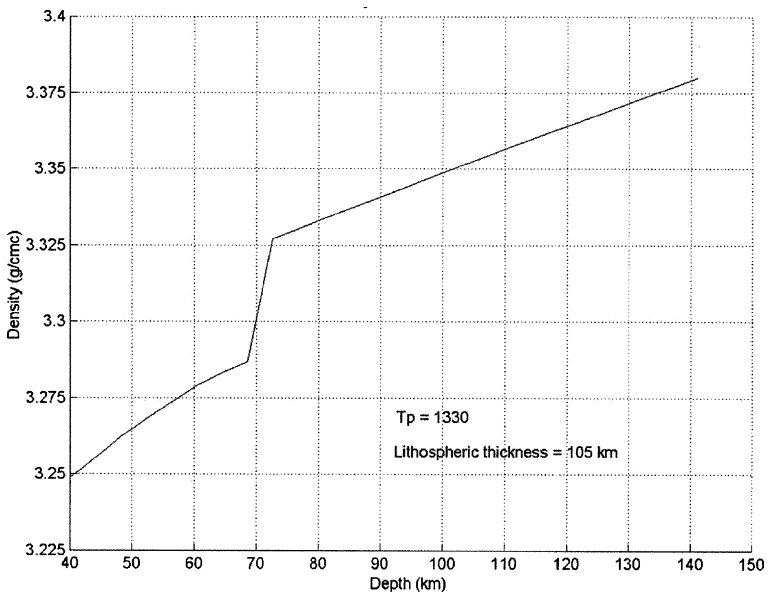

Fig. 6. Vertical density profile of the residual mantle rocks within the asthenosphere upwelling beneath the Tyrrhenian Basin; depth range: 140–40 km.

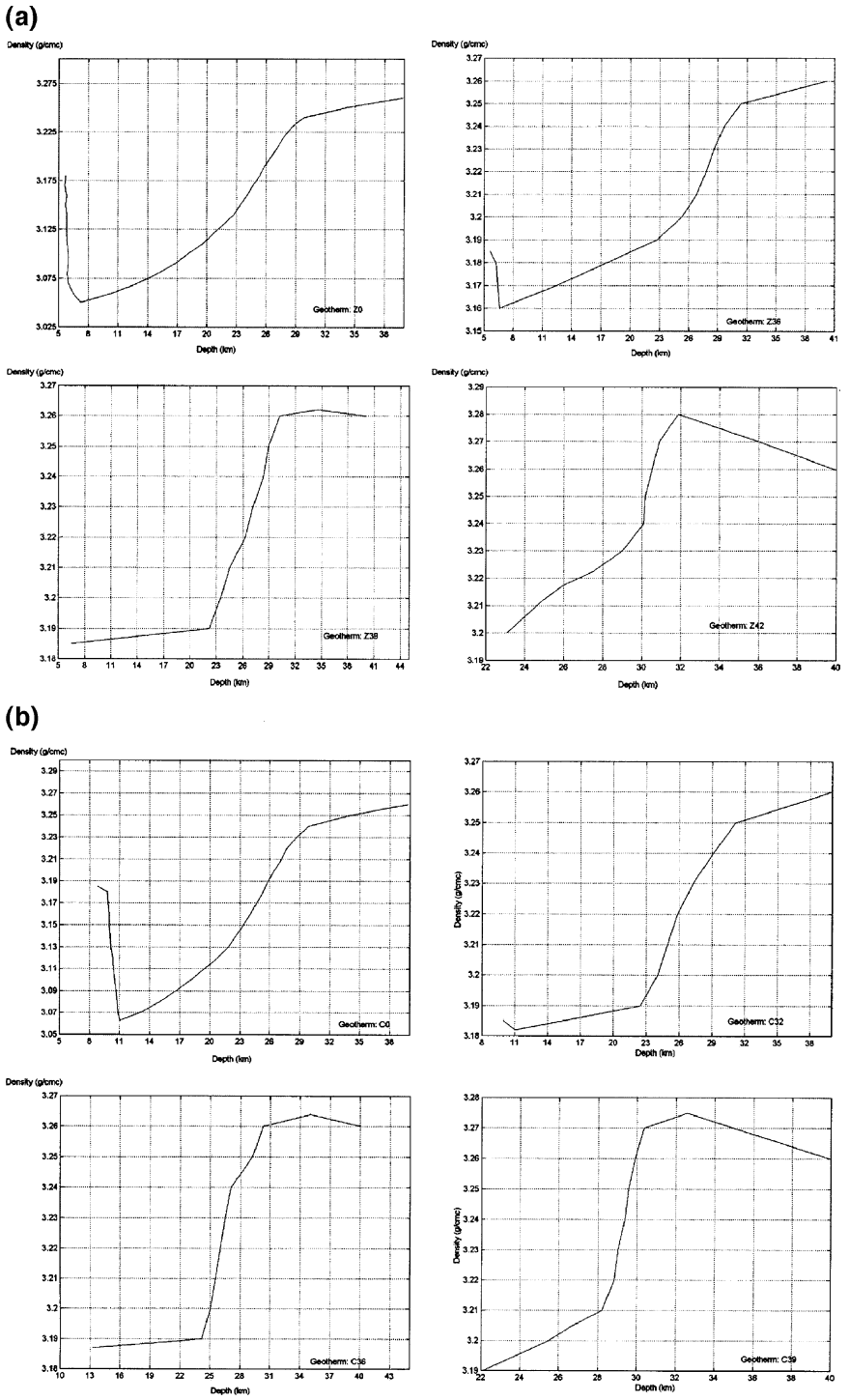

Fig. 7. Vertical density profile of the residual mantle rocks within the asthenosphere upwelling beneath the Tyrrhenian Basin; depths<40 km. Differences between (a) and (b): see the text.

(within the two small areas with the highest heat flow). Results confirm that each of the physical parameters considered has a specific control on the mantle density. Finally, density values provided by these computations were used to constrain the interpretation of the gravity data.

4. Temperature and density distribution in the sinking slab

The great closeness between the mantle uprise beneath the Tyrrhenian spreading axis, and the westward subduction of the African margin beneath the European plate, clearly means the existence of a contribution of the sinking slab to the gravity anomaly field of the Tyrrhenian basin. This contribution has to be computed and taken into account when gravity data are interpreted.

The Adriatic microplate subduction started in the late Oligocene–Early Miocene. At present, subduction of the Southern Adriatic sector of the plate is demonstrated by the existence of a well defined Benioff plane under the Tyrrhenian sea. Many authors (Gasparini, 1982; Anderson and Jackson, 1987; Guerra et al., 1991; Giardini and Velonà, 1991; Amato et al., 1993; Selvaggi and Chiarabba, 1995; Cimini, 1999; Selvaggi, 2001; Chiozzi et al., 2002) have defined the geometry of the subducted slab by different seismological methods. Selvaggi and Chiarabba (1995) have defined a continuous slab having a slope down to 50 km of depth, then a rapid increase at the hinge, where the slope reaches 70° that maintains constant down to 500 km. The thickness of the slab is about 80 km. By assuming a subduction age of 20 Ma, we deduce an average subduction rate of 2.5 cm/a. Temperature within the cold slab depends mainly on:

(i) heating by conduction from the hotter asthenosphere;
(ii) advection of heat in the moving slab;
(iii) heating by compression of the asthenosphere.

For (i) point, according to Devaux et al. (1997), we assume that the surrounding close mantle moves downward with the slab and heats adiabatically, as in the whole mantle; for (iii) point we retain that in steady state conditions the horizontal movement of the slab within a thermal fluid mantle horizontally stratified does not perturb the temperature in the slab.

Two other phenomena connected with the subduction are the corner flow and the slab retrait.

Minear and Toksoz (1970), McKenzie (1969, 1984), Devaux et al. (1997) have studied the problem by considering the factors (i) and (ii) by analytical or numerical methods. In this paper we studied all the effects by analytical methods.

Fig. 8 shows the reference system of our model and the slab, having a slope α with respect to the Earth surface.

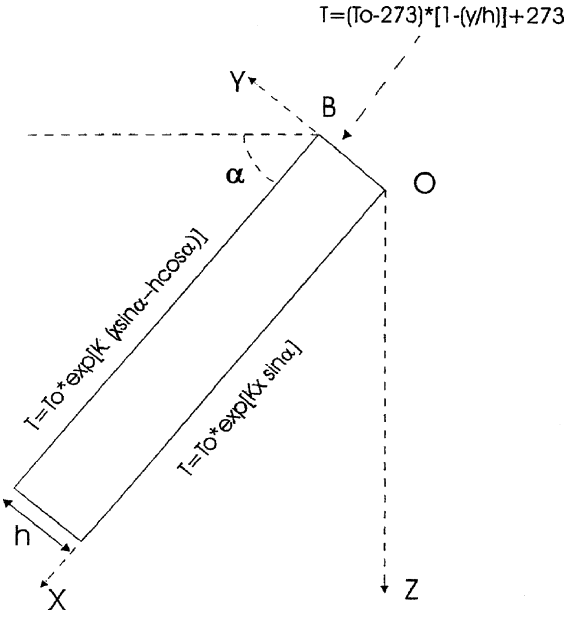

Fig. 8. Reference system of a subducting slab beneath the Tyrrhenian Sea.

The adiabatic gradient in the mantle (see e.g. Turcotte and Subert, 1982) is

$$\left(\frac{dT}{dz}\right)_s = \frac{\alpha_v g T}{C_p} \tag{1}$$

where T is the absolute temperature, α_v the coefficient of thermal expansion at constant volume, which is $3*10^{-5}$ K^{-1} for the upper mantle where the thermal gradient is about 0.5 K/km and about $2*10^{-5}$ K^{-1} for the deeper mantle where the gradient is about 0.3 K km^{-1} (Fowler, 1992; Devaux et al., 1997); here we assume an average value of $2.5 \cdot 10^{-5}$ K^{-1}. C_p (1 kJ kg^{-1} K^{-1}) is the specific heat at constant pressure, g (10 m/s^2) the gravity acceleration, z the vertical axis with respect to the Earth surface. From Eq. (1) we obtain by integration:

$$T = T_0 \exp(kz) \tag{2}$$

where T_0=1660 K is the temperature at the base of the lithosphere,

$$k = \frac{\alpha_v g}{C_p}. \tag{3}$$

Temperatures over the lower and upper surfaces of the slab are respectively:

$$T(x, y = 0) = T_0 \exp(kx \sin\alpha)$$

$$T(x, y = h) = T_0 \exp(kx \sin\alpha - kh \cos\alpha) \tag{4}$$

where h is the slab thickness and α the dipping angle.

We assume:

$$T(x=0,y)=(T_0-273)\left(1-\frac{y}{h}\right)+273 \qquad 0<y<h \tag{5}$$

over OB.

The energy balance equation within a two dimensional subducting slab in steady state is:

$$\lambda\left(\frac{\partial^2 T}{\partial x^2}+\frac{\partial^2 T}{\partial y^2}\right)-\rho C_p v\frac{\partial T}{\partial x}+\rho g v\alpha_{vs}T\sin\alpha=0 \tag{6}$$

where λ is the thermal conductivity ($Wm^{-1}\,{}^{\circ}K^{-1}$) v the subduction rate; the first term refers to the conduction, the second term to the advection and the third term to the compression. The solution to Eq. (6) with the above boundary conditions is shown in Appendix.

Fig. 9 shows the temperature distribution within the slab, assuming $h=80$ km, $\lambda=3.0$ $Wm^{-1}\,K^{-1}$, $\rho=3300$ kg m^{-3}. $\alpha_{vs}=2\cdot10^{-5}$ K^{-1} (because the slab is cooler than the mantle) $v=2.5$ cm/a, $\alpha=70^{\circ}$.

We can see that isotherms are dragged downward by the motion of the subducting slab. The inner section of the slab is cooler than the outer sectors, indicating that the advection is dominant, even though it is reduced by the heat generated by compression.

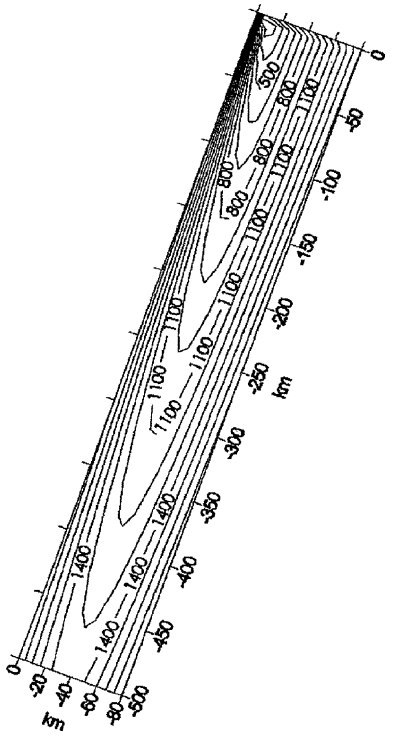

Fig. 9. Temperature within the subducting slab (in K).

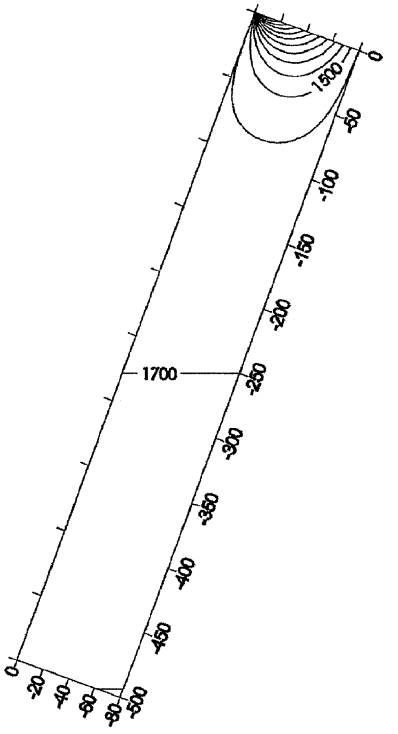

Fig. 10. Predicted temperature (in K) within a subducted slab at rest.

By putting $v=0$ in Eq. (6) we obtain:

$$\left(\frac{\partial^2 T}{\partial x^2}+\frac{\partial^2 T}{\partial y^2}\right)=0. \tag{7}$$

The solution to this equation with the same boundary conditions (Eq. (4)) is easily obtained by putting $v=0$ in the solution to Eq. (6). This gives the temperatures of the slab at rest. Fig. 10 shows the calculated isotherms.

The upper part of the slab is cold depending on the surface conditions. In the inner part the temperature is equal to that of the mantle.

By subtracting the solution to Eq. (6) from the solution to Eq. (7) we obtain the temperature difference (negative) between the slab and the mantle. Fig. 11 shows the resulting isotherms.

We see that the slab is colder than the mantle. Highest negative anomalies are almost superficial and internal. They are also asymmetrical.

From the distribution of ΔT within the slab, by using the equation:

$$\rho(T)=\rho_0(1-\alpha_v\Delta T)$$

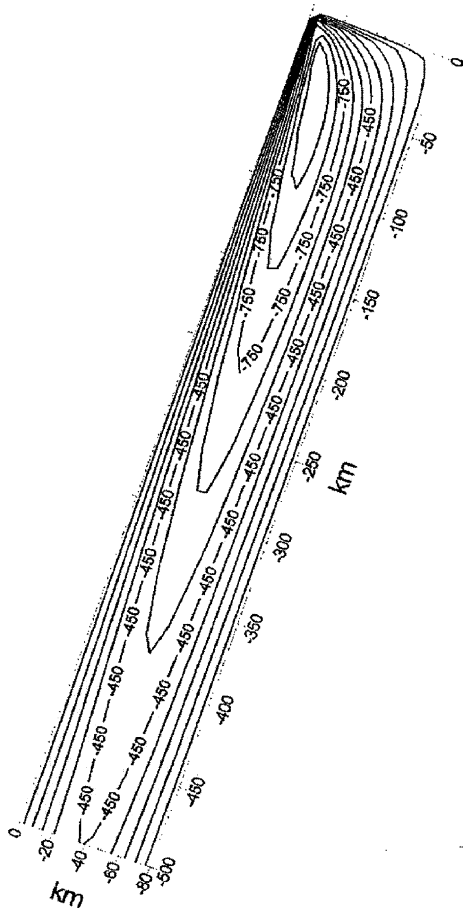

Fig. 11. Difference between temperature (in K) within the slab and the surrounding mantle.

we can obtain the density anomalies of the slab with respect to the mantle:

$$\Delta\rho = \rho_0 - \rho(T) = \rho_0 \alpha_v \Delta T.$$

Fig. 12 shows that maximum density anomaly is internal and it decreases with depth. The density anomaly ranges from 30 to 60 kg/m^3 in the upper part of the slab.

At about 400 km of depth there is a density increase of about 270 kg/m^3 associated with the transformation of the olivine to a spinel structure.

In evaluating the density and temperature variations due to this transition we follow Turcotte and Subert (1982). The olivine–spinel phase boundary is elevated in the sinking slab compared to its position in the surrounding mantle because the pressure at which the phase change occurs depends on the temperature. The shape of the boundary transition is given in the $(z(p),T)$ plane by the Clapeyron curve (Turcotte and Subert, 1982):

$$z = h_{0_s} = \frac{\gamma \Delta T}{\rho g}$$

where γ is the slope of the (p,T) curve:

$$\gamma = \frac{dp}{dT}$$

and ΔT the difference between the temperature in the slab at 410 km of depth and the temperature in the surrounding mantle at the same depth.

Since dT is negative for lower temperatures in the interior of the descending lithosphere and $\gamma > 0$, dz is also negative, so that the olivine to spinel phase change occurs at shallower depth in the mantle. With the parameters given in the text we have estimated a maximum uplift of about 33–35 km of the phase boundary in the Tyrrhenian slab.

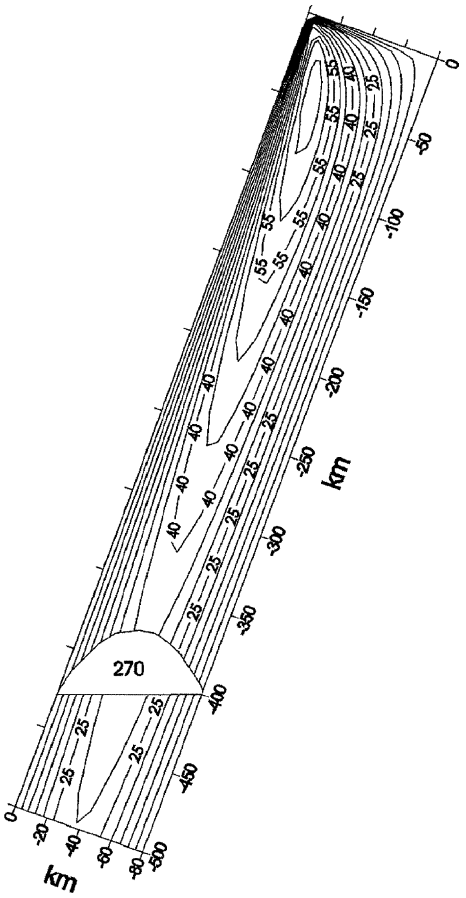

Fig. 12. Excess density distribution within the slab with respect to the density of the mantle. White sector refers to the denser spinel phase.

5. Gravity modelling: data discussion and interpretation

Because of the aim of the study, essentially limited to deep and large scale structures, the data interpretation concerned only the regional component of the gravity profile.

Several studies indicate that gravity anomalies due to Moho geometry have at least a wavelength of some hundreds of kilometers (Pinna and Rapolla, 1979; Cella et al., 1995). Nevertheless, the presence of strong variations of the Moho depth along small distances (with depths from 30 km up to 10 km in the Tyrrhenian Basin) suggested the choice of a smaller cut-off wavelength (100 km) (Fig. 13).

Data were prior tapered with a maximum entropy predictor algorithm to prevent distortions from boundary effects. Long wavelength components were selected by means of a frequency domain filter provided with a Hamming–Tukey window.

Therefore, the gravity effect due to density discontinuities within the shallow crust (including the effect due to the unavoidable choice of a unique density value for the terrain correction, even if in the presence of lateral variations within the masses beneath the topography) was completely removed from the interpreted profile. The sole intra-crustal feature generating a long period gravity signal is the lateral transition between "oceanic" and continental crust and, therefore, it was modelled basing on seismic data (Duschenes et al., 1986).

The regional gravity anomaly field was interpreted along a profile WNW–ESE oriented for a length of about 850 km. The profile covers the whole Tyrrhenian Basin, crossing the Sardinia plate and the Calabrian Arc, respectively, toward NW and SE.

Data were interpreted adopting a technique that resolves the 2.5 D inverse problem of determining the density contrast function and the source top and bottom functions from the measured data sets by using the spectral expansion linear inverse problem (e.g. Fedi, 1989). Because of the non-linearity of the problem, linearization is assumed and the Frechet derivatives of the data functionals with respect to the density and to the source top and bottom depths are calculated. The algorithm is very efficient and only a few iterations are required to reach a good convergence error.

Several reliable information were introduced in the modeling as constraints. Reasonable half-strike values was set for every body source as in Table 1, taking into account the presumable extension of main structures crossed along the direction normal with respect to the profile.

The thickness of the lithosphere in the continental regions surrounding the Tyrrhenian Basin (Sardinia and Calabria) were partially constrained with data from several authors (Knopoff and Panza, 1978; Panza et al., 1980; Calcagnile and Panza, 1981; Suhadolc and

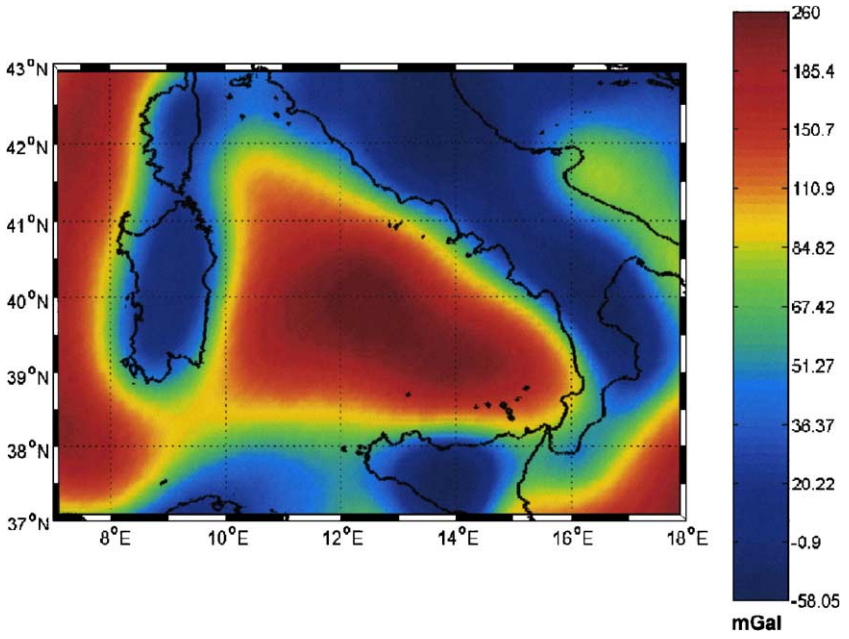

Fig. 13. Regional Bouguer anomaly field of the Tyrrhenian Basin. Low-pass filter; cut-off wavelength = 100 km; step grid = 5′.

Table 1
Half strike values chosen for 2.5 inversion along the given profile

Continental crust	Oceanic crust	Lithospheric mantle	Upwelling asthenosphere
150 km	150 km	350 km	From 350 km to 80 km (upward)

Panza, 1989) and based on the dispersion of the Rayleigh-waves. An average value of density typical of the continental lithotypes (2.85 g/cm^3), was assigned basing on many previous works as described in Cella et al. (1995). The model does not consider the hypothesis of asthenospheric material directly underlying the crust beneath the Calabrian Arc (Gvirtzman and Nur, 1999) since there are no evidences of somewhat related magmatism that should be expected at crustal depths by adiabatic decompression of asthenospheric material.

Data from seismic investigations (Finetti and Morelli, 1972; Steinmetz et al., 1983; Recq et al., 1984; Duschenes et al., 1986; Nicolich, 1989; Scarascia et al., 1994) and from heat flow studies (Della Vedova et al., 1984) indicate, for the central area of the Tyrrhenian depression, a crustal thickness of about 8–10 km. These information were used to constrain the Moho depth along the profile. Data reported by Duschenes et al. (1986), concerning the geographic extent of the "oceanic" crust (~300 km along the profile), were adopted in our case.

However, the transition from continental to "oceanic" crust in the Tyrrhenian Basin is a still debated argument because in the Tyrrhenian central area some authors (Thisseau et al., 1986) individuate only extremely stretched and fragmented continental crust, diffusely intruded by oceanic material and still representing a noticeable portion of the whole crustal volume. Thus, it is reasonable to attribute to this crustal segment features intermediate between continental and oceanic crust. Therefore a density of 2.85 g/cm^3 was assigned to the crustal rocks surrounding the two central sectors of the Vavilov and Marsili Basins, in correspondence of the two main positive heat flow anomalies. Here the crustal thinning reaches the higher values and a prevailing presence of basalt dykes is instead probable. Consequently, a slightly higher density (2.9 g/cm^3) has been chosen for these areas.

Other two significant sets of information were adopted to reduce the ambiguity of the gravity interpretation. With the first one, the model was constrained by introducing the information (see Section III) represented by the vertical distribution of density within the

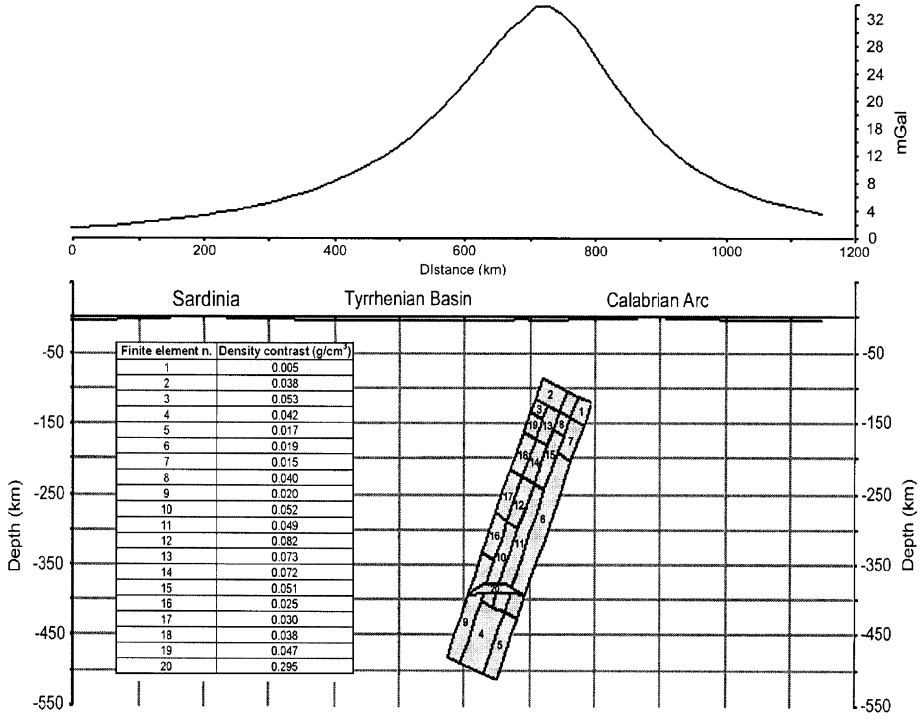

Fig. 14. 2D regional gravity profile showing the long wavelength contribution of a finite element model reproducing the subducting slab beneath the eastern part of the Tyrrhenian Basin.

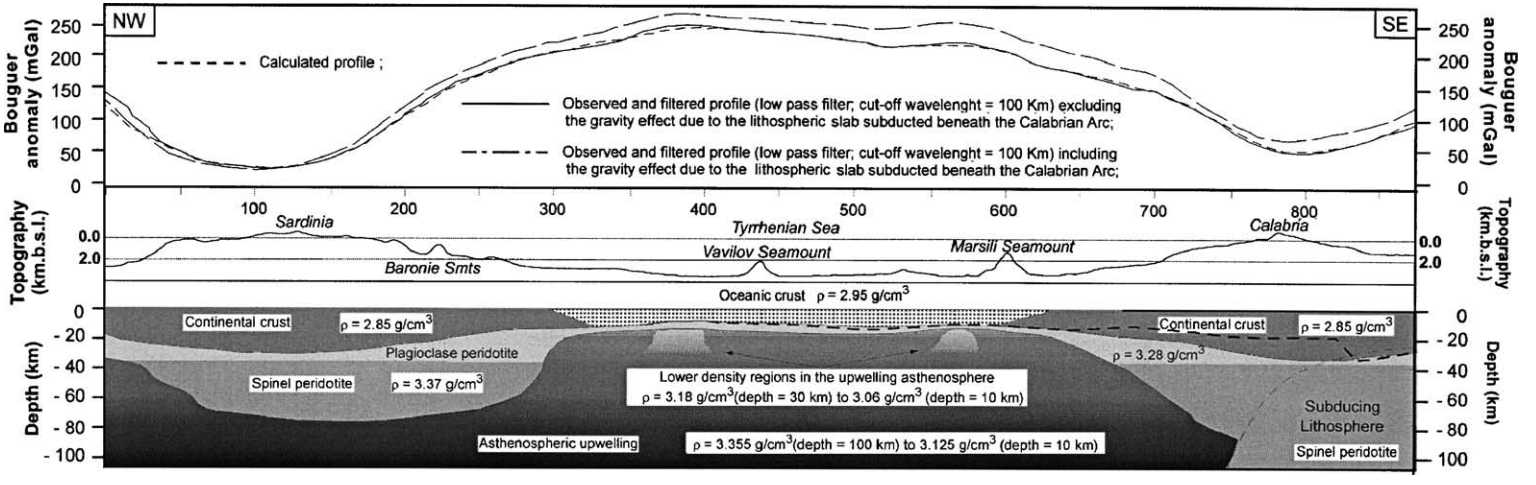

Fig. 15. Regional gravity model of the litho–asthenospheric structure along the interpreted profile; the dashed line indicates the moho depth beneath the Calabrian Arc as predicted by Scarascia et al. (1994).

rising mantle as computed by petro-physical criteria from laboratory evidences. Variations were discretized by modeling the upwelling asthenosphere as a set of layers 10 km thick and by assigning to each layer the value computed for its intermediate depth. Averaged densities of 3.4, 3.37, and 3.28 g/cm^3 were assigned, respectively, to the garnet (more than 110 km of depth), spinel (depths from 75 to 35 km), and plagioclase peridotite (less than 35 km of depth). Densities gradually ranging from 3.35 g/cm^3 (at a depth of 100 km) to 3.06 g/cm^3 (at a depth of 15 km) were assigned to the rising mantle.

The second constraint was imposed to the interpretation by assigning the density values previously computed (see Section IV) to the finite element model reproducing the slab sinking beneath the Tyrrhenian Basin (Fig. 14). The range of densities predicted within the slab model is very broad (up to 0.29 g/cm^3) and represents a mass excess within the upper mantle, thus generating a significant long wavelength positive anomaly with the maximum (about 35 mGal of amplitude) located beneath the eastern part of the Tyrrhenian Basin, between the Marsili Seamount and the coast of Calabria (Fig. 14). The gravity contribution of the finite element model reproducing the subducting slab was subtracted from the measured gravity profile. Afterwards, the resulting profile was interpreted as in Fig. 15.

6. Conclusions

The structural model resulting from the interpretation of gravity data along the chosen profile (Fig. 15) provides an image of the main litho-asthenospheric sources by introducing both constraints from other geophysical evidences and from results of petro-physical computations based on heat flow studies and on experimental data concerning the physical properties of the uppermost mantle. However, the gravity modelling here presented introduces new significant constraining elements with respect to previous studies (Cella et al., 1998).

Firstly, the computation of the density distribution within the Tyrrhenian asthenosphere has been based on new geotherms predicted by a re-interpretation of the heat flow anomalies in this area.

Second, the interpretation of the gravity profile accounts also for the gravity contribution of the lithospheric slab subducting within the upper mantle beneath the Tyrrhenian Basin. To do this, the temperature distribution within the sinking plate was modelled not only basing, as already done for previous models, on (a) the heating by conduction from the hotter asthenosphere and (b) the advection of heat in the moving slab, but also (c) accounting for the heating by compression of the asthenosphere.

The satisfactory agreement between measured and computed gravity data depicts a structural and geodynamic outline at regional scale with several interesting elements.

The crustal thickness beneath the Sardinia microplate reaches about 30 km in correspondence of the areas of highest topography. As previously evidenced (Cella et al., 1998), the lithospheric roots of the Sardinia plate with greater thickness (about 85 km) appears instead to be shifted to the east. This could reinforce the hypothesis of an underlying eastward migrating asthenosphere (Doglioni et al., 1998).

Moho gradually rises toward the Tyrrhenian Basin, reaching shallower depths ($\approx$ 25 km) beneath the Tyrrhenian coast of Sardinia, westward, and of Calabria, eastward, up to a minimum depth (9–10 km) beneath the Tyrrhenian bathial plain.

Toward the central sector of the Tyrrhenian Basin, the LAB abruptly rises up to depths of about 12 km beneath the central bathial plain, confirming an intense stretching of the continental lithosphere ($\beta \approx 6$) and a strong modification of its structure. Here, in fact, the lithospheric boudinage occurring by means of a jumping process of the spreading centers appears discontinuous both in space and time and clearly indicates an eastward migrating mantle upwelling. The latter is caused not only by the extensional regime due to external driving forces, induced by the slab pull (Forsyth and Uyeda, 1975; Angelier and Le Pichon, 1979), but also appears reinforced by the mantle flow triggered by the eastward rollback of the westward subducting slab (McKenzie, 1969; Turcotte and Subert, 1982; Marotta and Mongelli, 1998) and by the advection of the asthenosphere beneath the LID toward the subduction zone (Toksoz and Hsui, 1978). The computations confirm that the mantle potential temperature exceed only a few tens of degrees Centigrade (°C) ($T_p \approx 1330$ °C) with respect to the normal conditions. However, a large amount (up to 20%) of mantle rocks melts and migrates upward, partly at the earth surface, as basaltic magmas, and partly as underplating igneous basic rocks at the base of the thinned crust. Its original structure is therefore reduced to isolated crystalline relicts sparse within small “ocean” like spreading centres in correspondence of the Tyrrhenian bathial plain.

Eastward, the gravity model depicts a crustal structure of the Calabrian accretionary wedge rather different with respect to those suggested in the last years

(Scarascia et al., 1994). In fact, instead of an abrupt increase in thickness delineating a crustal decoupling, the Moho seems to gently deepens up to a reach of 35 km beneath the Ionian side of the Calabria arc. Beneath the western side of the chain, in correspondence of the subduction hinge the lithosphere thickens up to 85 km. Here, the interpretation of the gravity data accounts also for the gravity effect due to the plate sinking beneath the Calabrian Arc. It consists of a very long wavelength positive anomaly with an amplitude of about 35 mGal. This contribution has been computed starting from a density model that hypothesizes an 80 km thick plate subducting with an angle of about 70°, with subduction rates of 2–3 cm y^{-1}, that is a value smaller than suggested by other studies.

Acknowledgements

C. Doglioni is thanked for frequent discussions and constructive comments concerning the argument discussed here.

Appendix A

A.1. Solution of heat Eq. (6)

By putting:

$$\delta = \frac{\rho g v \alpha_{vs} \sin\alpha}{\lambda} \qquad \beta = \frac{\rho C_p v}{\lambda}. \tag{A7}$$

Eq. (6) becomes:

$$\left(\frac{\partial^2 T}{\partial x^2} + \frac{\partial^2 T}{\partial y^2}\right) - \beta \frac{\partial T}{\partial x} + \delta T = 0. \tag{A8}$$

If we consider the following non-dimensional variables:

$$\begin{cases} T' = T/T_0 & \text{(A9a)} \\ x' = x/h & \text{(A9b)} \\ y' = y/h & \text{(A9c)} \end{cases}$$

Eq. (A8) can be written as:

$$\left(\frac{\partial^2 T'}{\partial x'^2} + \frac{\partial^2 T'}{\partial y'^2}\right) - \beta' \frac{\partial T'}{\partial x'} + \delta' T' = 0 \tag{A10}$$

where:

$$\delta' = \delta h^2 \qquad \beta' = h\beta \tag{A11}$$

The boundary conditions (4) and (5) in the non-dimensional variables can be written as follows:

$$\begin{cases} T'(x', y' = 0) = \exp(khx' \sin\alpha) & \text{(A12a)} \\ T(x', y' = 1) = \exp kh(x' \sin\alpha - \cos\alpha) & \text{(A12b)} \\ T(x' = 0, y') = \left(1 - \frac{273}{T_0}\right)(1 - y') + \frac{273}{T_0} & 0<y'<1. \end{cases}$$

(A12c)

The solution to Eq. (A10) is given by the sum:

$$T' = T'_{\mathrm{g}} + T'_{\mathrm{P}} \tag{A13}$$

where T'_{g} is the general integral of Eq. (A10) and T'_{P} is a particular solution to the same equation.

A.2. The particular solution

Let us first search a particular solution T'_{P}. Assume that:

$$T'_{\mathrm{p}}(x', y') = f(x')g(y'). \tag{A14}$$

By substituting Eq. (A14) in Eq. (A10) we obtain:

$$\begin{cases} \frac{f''}{f} - \beta' \frac{f'}{f} = \gamma & \text{(A15a)} \\ -\left[\frac{g''}{g} + \delta'\right] = \gamma & \text{(A15b)} \end{cases}$$

where γ is a constant. If we assume:

$$f(x') = \exp(khx' \sin\alpha) \tag{A16}$$

by substituting Eq. (A16) in Eq. (A15a) the constant is found to be:

$$\gamma = k^2 h^2 \sin^2\alpha - \beta' kh \sin\alpha. \tag{A17}$$

Moreover, by using Eq. (A14), the two boundary conditions Eqs. (A12a,b) are satisfied only if:

$$g(0) = 1 \tag{A18}$$

and:

$$g(y' = 1) = \exp(-kh\cos\alpha) \tag{A19}$$

So, the solution to Eq. (A15b) must satisfy the boundary conditions (A18) and (A19).

If we assume:

$$\psi^2 = \gamma + \delta' \tag{A20}$$

the Eq. (A15b) becomes:

$$\frac{g''}{g} = -\psi^2. \tag{A21}$$

Three different solutions could give according to the sign of ψ^2. In our case, by assuming: $h=80$ km, $\lambda=3$ Wm^{-1} K^{-1}, $\rho=3300$ kg/m^3, $\alpha_{vs}=2\times10^{-5}$ K^{-1}, $v=2.5$ cm/a, $\alpha=70^\circ$, $\psi^2>0$. In this case, the solution to Eq. (A21) is given by:

$$g(y') = A\cos(\psi y') + B\sin(\psi y'). \tag{A22}$$

From the conditions (A18) and (A19) it follows that:

$$A = 1 \tag{A23}$$

and:

$$B = \frac{\exp(-kh\cos\alpha) - \cos\psi}{\sin\psi}. \tag{A24}$$

By substituting Eqs. (A23) and (A24) in Eq. (A22), it follows that:

$$g(y') = \cos(\psi y') + \left[\frac{\exp(-kh\cos\alpha) - \cos\psi}{\sin\psi}\right]\sin(\psi y'). \tag{A25}$$

By taking into account Eqs. (A14), (A16), and (A25), the particular solution to the heat equation, for the case $\psi^2>0$, is given by:

$$T'_p(x',y') = \exp(khx'\sin\alpha) \times \left[\cos(\psi y') + \left(\frac{\exp(-kh\cos\alpha)-\cos\psi}{\sin\psi}\right) \times \sin(\psi y')\right]. \tag{A26}$$

A.3. The general solution

The general integral to Eq. (A10) can be written as:

$$T'_g(x',y') = \sum_{n=1}^{\infty} T_n = \sum_{n=1}^{\infty} A_n\sin(n\pi y')\exp(\alpha_n x') \tag{A27}$$

with the coefficients α_n to be determined. The sinusoidal dependence on y' assures that the series Eq. (A27) assumes nil values on both $y'=0$ and $y'=1$. This implies that the two boundary conditions (A12a,b) are satisfied by the solution (A13). In Eq. (A27) the series coefficients A_n must be determined by imposing the boundary condition (A12c), as we show in the next sections.

In order to determine the α_n coefficients we substitute Eq. (A27) in Eq. (A10). It follows that:

$$\begin{aligned} &A_n\alpha_n^2\sin(n\pi y')\exp(\alpha_n x') \\ &- (n\pi)^2 A_n\sin(n\pi y')\exp(\alpha_n x') \\ &- \beta' A_n\alpha_n\exp(\alpha_n x')\sin(n\pi y') \\ &+ \delta' A_n\sin(n\pi y')\exp(\alpha_n x') \\ &= 0. \end{aligned} \tag{A28}$$

Eq. (A28) is equivalent to:

$$\alpha_n^2 - \beta'\alpha_n - (n\pi)^2 + \delta' = 0. \tag{A29}$$

The only physically acceptable solution to Eq. (A29) is:

$$\alpha_n = \frac{\beta'}{2} - \sqrt{\frac{\beta'^2}{4} - \delta' + n^2\pi^2}. \tag{A30}$$

A.4. The complete solution

By summing Eqs. (A26) and (A27) the complete solution to Eq. (A10), is given by:

$$T' = T_g' + T_P' = \exp(khx'\sin\alpha) \times \left[\cos(\psi y') + \left(\frac{\exp(-kh\cos\alpha) - \cos\psi}{\sin\psi}\right) \times \sin(\psi y')\right] + \sum_{n=1}^{\infty} A_n\sin(n\pi y')\exp(\alpha_n x'). \tag{A31}$$

The A_n coefficients can be determined by imposing the boundary condition (A12c), from which it follows that:

$$\sum_{n=1}^{\infty} A_n\sin(n\pi y') = \left(1 - \frac{273}{T_0}\right)(1-y') + \frac{273}{T_0} - \left[\cos(\psi y') + \left(\frac{\exp(-kh\cos\alpha) - \cos\psi}{\sin\psi}\right) \times \sin(\psi y')\right] \tag{A32}$$

or:

$$A_n = 2\int_0^1 \left\{\left(1 - \frac{273}{T_0}\right)(1-y') + \frac{273}{T_0} - \left[\cos(\psi y') + \left(\frac{\exp(-kh\cos\alpha) - \cos\psi}{\sin\psi}\right) \times \sin(\psi y')\right]\right\}\sin n\pi y' y'. \tag{A33}$$

The integrals in Eq. (A33) can be easily computed. The result is:

$$A_n = \frac{2}{n\pi}\left\{1-\frac{273}{T_0}(-1)^n\right\}+\left[\frac{1}{\psi+n\pi}(\cos(\psi+n\pi)-1)\right.$$
$$\left.-\frac{1}{\psi-n\pi}(\cos(\psi-n\pi)-1)\right]+$$
$$-\frac{\exp(-kh\cos\alpha)-\cos\psi}{\sin\psi}$$
$$\times\left[\frac{1}{\psi-n\pi}\sin(\psi-n\pi)-\frac{1}{\psi+n\pi}\sin(\psi+n\pi)\right] \quad \text{(A34)}$$

References

Abbate, E., Bortolotti, V., Passerini, P., Principe, G., Treves, B., 1994. Oceanization processes and sedimentary evolution of the Northern Apennine ophiolitic suite: a discussion. Mem. Soc. Geol. Ital. 48, 117–136.

Alvarez, W., 1972. Rotation of the Corsica–Sardinia microplate. Nature 235, 103–105.

Amato, A., Cimini, G.B., Alessandrini, B., 1991. Struttura del sistema litosfera-astenosfera nell'Appennino settentrionale da dati di tomografia sismica. Studi Geolog. Camerti, Vol. Spec. 1991/1, 83–90.

Amato, A., Alessandrini, B., Cimini, G., Frepoli, A., Selvaggi, G., 1993. Active and remnant subducted slabs beneath Italy: evidence from seismic tomography and seismicity. Ann. Geofis. 26, 201/214.

Anderson, H., Jackson, J., 1987. The deep seismicity of the Tyrrhenian Sea. Geophys. J. R. Astron. Soc. 91, 613–637.

Angelier, J., Le Pichon, X., 1979. The Hellenic Arc and Trench system: a key to the tectonic evolution of the eastern Mediterranean. Tectonophysics 60, 1–40.

Beccaluva, L., Bonati, E., Dupuy, C., et al., 1990. Geochemistry and mineralogy of volcanic rocks from the ODP sites 650, 651, 655 and 654 in the Tyrrhenian sea. Proceeding of the ODP. Scientific Results, vol. 107, pp. 49–74.

Boccaletti, M., Elter, P., Guazzone, G., 1971. Plate tectonics model for development of the western Alps and northern Apennines. Nature 234, 108–111.

Calcagnile, G., Panza, G.F., 1981. The main characteristics of the lithosphere asthenosphere system in Italy and surrounding regions. Pageoph 119, 865–879.

Caputo, M., Panza, G.F., Postpischel, D., 1970. Deep structure in the Mediterranean basins. J. Geophys. Res. 75, 4919–4923.

Cataldi, R., Mongelli, F., Squarci, P., Taffi, L., Zito, G., Calore, C., 1995. Geothermal ranking of Italian territory. Geothermics, No. 1, pp. 115, 129.

Cella, F., Rapolla, A., 1997. Density changes in upwelling mantle. Phys. Earth Planet. Inter. 103 (1-2), 63–84.

Cella, F., Dorre, A.S., Rapolla, A., 1995. Moho and lithosphere–asthenosphere boundary in East Africa from regional gravity data. Boll. Geofis. Teor. Appl. XXXVII (148), 277–301.

Cella, F., Fedi, F., Florio, G., Rapolla, A., 1998. Optimal gravity modelling of the litho–asthenosphere system in Central Mediterranean. Tectnophysics 287 (1-4), 117–138.

Cherchi, A., Montadert, L., 1982. Oligo-miocene rift of Sardinia and the early history of the west mediterranean basin. Nature 298, 736–739.

Chiozzi, P., Pasquale, V., Verdoya, M., 2002. Thermal constrains to the geodynamic processes in the Southern Tyrrhenian. Atti 21 Conv. Gruppo Nazionale Geofisica Terra Solida. GNGTS-CNR, Roma, pp. 1–8.

Cimini, G.B., 1999. P-wave deep velocity structure of the Southern Tyrrhenian Subduction Zone from nonlinear traveltime tomography. Geophys. Res. Lett. 26, 3709–3712.

Corrado, G., Rapolla, A., 1981. The gravity field of Italy: analysis of its spectral composition and delineation of a tridimensional crustal model for central-southern Italy. Boll. Geofis. Teor. Appl. 23, 17–29.

Courtney, R.C., White, R.S., 1986. Anomalous heat flow and geoid across the Cape Verde rise: evidence of dynamic support from a thermal plume in the mantle. Geophys. J. R. Astron. Soc. 87, 815–868.

Cucci, L., Cinti, F., 1999. Regional uplift and local tectonic deformation recorded by the Quaternary marine terraces in the Ionian coast of northern Calabria (southern Italy). Tectonophysics 292, 67–83.

Decourt, J., Zonenshain, L.P., Ricou, L.E., et al., 1986. Geological evolution of the Tethis belt from the Atlantic to the Pameirs since the Lias. Tectonophysics 123, 241–315.

Della Vedova, B., Pellis, G., Foucher, J.P., Rehault, J.-P., 1984. Geothermal structure of the Tyrrhenian Sea. Mar. Geol. 55, 271–289.

Devaux, J.P., Schubert, G., Anderson, C., 1997. Formation of a metastable olivine wedge in a descending slab. J. Geophys. Res. 102, 24627–24637.

Doglioni, C., 1991. A proposal of kinematic modelling for W-dipping subductions—possible applications to the Tyrrhenian–Appennines system. Terra Nova 3, 423–434.

Doglioni, C., Mongelli, F., Pialli, G.P., 1998. Boudinage of the Alpine belt in the Apenninic back-arc. Mem. Soc. Geol. Ital. 52, 447–468.

Doglioni, C., Gueguen, E., Harabaglia, P., Mongelli, F., 1999. On the origin of west-directed subduction zones and application to the western Mediterranean. In: Durand, B., Jolivet, L., Horvath, F., Seranne, M. (Eds.), The Mediterranean basins: tertiary extension within the Alpine orogen, Geological Soc., London, special publications 156, pp. 541–561.

Duschenes, J., Louden, K.E., Sinha, M.C., 1986. A seismic refraction experiment in the Tyrrenhian Sea. Geophys. J. R. Astron. Soc. 85, 139–160.

Faccenna, C., Thorsten, W. Becker, Lucente, F.P., Jolivet, L., Rossetti, F., 2001. History of subduction and back arc extension in the Central Mediterranean. Geophys. J. Int. 145 (3), 809.

Fallon, T.J., Green, D.H., 1987. Anhydrous partial melting of MORB pyrolite and other peridotite compositions at 10 kbar: implications for the origin of MORB glasses. Mineral. Petrol. 37, 181–219.

Fedi, M., 1989. Spectral expansion inversion of gravity data for 2.5 D structures. Boll. Geofis. Teor. Appl. XXXI (121), 25–39.

Finetti, M., Del Ben, A., 1986. Geophysical study of the Tyrrhenian opening. Boll. Geofis. Teor. Appl. 28, 75–156.

Finetti, I., Morelli, C., 1972. Wide scale digital seismic exploration of the Mediterranean Sea. Boll. Geofis. Teor. Appl. XIV (56), 291–342.

Forsyth, D., Uyeda, S., 1975. On the relative importance of the driving forces of plate motions. Geophys. J. R. Astron. Soc. 43, 163–200.

Fowler, C.M.R., 1992. The Solid Earth. Cambridge University Press. 472 pp.

Gasparini, P., 1982. Seismo-tectonics of the Calabrian Arcs. Tectonophysics 84, 267–286.

Giardini, D., Velonà, M., 1991. The deep seismicity in the Tyrrhenian Sea. Terra Nova 3, 57–64.
Green, D.H., 1991. The Earth's lithosphere and asthenosphere—concepts and constraints derived from petrology and high pressure experiments. Geol. Soc.Aust. Spec. Publ. 17, 1–22.
Gueguen, E., Doglioni, C., Fernandez, M., 1997. Lithosphere boudinage in the western Mediterranean back-arc basins. Terra Nova 9 (4), 184–187.
Guerra, I., Currà, F., Moretti, A., 1991. Sull'attendibilità della localizzazione dei microterremoti intermedi e profondi nel Tirreno Sud-orientale. Atti 10 Comv. Nazionale Geofisica Terra Solida. GNGTS-CNR, Roma, pp. 95–106.
Gvirtzman, Z., Nur, A., 1999. Plate detachment, asthenosphere upwelling, and topography across subduction zones. Geology, 563–566 (June).
Hutchison, I., Von Herzen, R.P., Louden, K.E., Sclater, J.G., Jemsek, J., 1985. Heat flow in the Balearic and Tyrrhenian basins, Western Mediterranean. J. Geophys. Res. 90, 685–702.
Kastens, K., Mascle, J., Auroux, C., Bonatti, E., Broglia, C., Channell, J., Curzi, P., Emeis, K.C., Glacon, G., Asegawa, S., Hieke, W., Mascle, G., McCoy, F., McKenzie, J., Mendelson, J., Muller, C., Réhault, J.P., Robertson, A., Sartori, R., Sprovieri, R., Torii, M., 1988. ODP Leg 107 in the Tyrrhenian Sea: insights into passive margin and back-arc basin evolution. Geol. Soc. Amer. Bull. 100, 1140–1156.
Keen, C.E., 1985. The dynamics of rifting deformation of the lithosphere by active and passive driving forces. Geophys. J. R. Astron. Soc. 80, 95–120.
Knopoff, L., Panza, G.F., 1978. Resolution of upper mantle structure using higher modes of Rayleigh waves. Ann. Geophys. 30, 491–505.
Locardi, E., Nicolich, R., 1988. Geodinamica del Tirreno e dell' Appennino centro-meridionale: la nuova Moho. Mem. Soc. Geol. It. 41, 121–140.
Malinverno, A., 1981. Quantitative estimates of age and Messinian paleobathymetry of the Tyrrhenian Sea after seismic reflection, heat flow and geophysical models. Boll. Geofis. Teor. Appl. 23, 159–171.
Malinverno, A., Ryan, W.B.F., 1986. Extension in Tyrrhenian Sea and shortening in the Appennines as a result of arc migration driven by sinking of the lithosphere. Tectonics 5 (2), 227–245.
Marotta, A., Mongelli, F., 1998. Flexure of subducted slabs. Geophys. J. Int. 132, 701–711.
McKenzie, D., 1969. Speculation on the consequences and causes of plate motion. Geophys. J. R. Astron. Soc. 18, 1–32.
McKenzie, D., 1978. Some remarks on the development of sedimentary basins. Earth Planet. Sci. Lett. 40, 25.
McKenzie, D., 1984. The generation and compaction of partially molten rock. J. Petrol. 25, 713–765.
McKenzie, D., Bickle, M.J., 1988. The volume and composition of melt generated by extension of the lithosphere. J. Petrol. 29, 625–679 (Part. 3).
Menke, W., 1984. Geophysical data analysis: discrete inverse theory. Academic Press, New York. 260 pp.
Minear, J.W., Toksoz, N.M., 1970. Thermal regime of downgoing slab and global tectonics. J. Geophys. Res. 75, 1397–1419.
Mongelli, F., Zito, G., 2000. The thermal field in a basin after a sudden passive pure shear lithospheric extension and sublithospheric mechanical erosion: the case of the Tuscan basin (Italy). Geophys. J. Int. 142, 142–150.
Mongelli, F., Zito, G., Della Vedova, B., Pellis, G., Squarci, P., Taffi, L., 1991. Geothermal regime of Italy and surrounding seas. Exploration of the Deep Continental Crust. Springer-Verlag, Berlin, pp. 381–394.
Morelli, C., 1970. Physiography, gravity and magnetism of the Tyrrhenian Sea. Boll Geofis. Teor. Appl. XII (48), 275–311.
Morelli, C., 1995. Ulteriori vincoli, geofisici, petrografici e geodetici alla geodinamica del Mediterraneo centrale. Atti XIII, Conv. Naz. del GNGTS 1, pp. 27–43.
Morelli, C., Pisani, M., Gantar, C., 1975. Geophysical anomalies and tectonics in the Strait of Sicily and of the Ionian Sea. Boll. Geofis. Teor. Appl. XVII (67), 211–249.
Nicolich, R., 1989. Crustal structures from seismic studies in the frame of the European Geotraverse (Southern segment) and CROP projects. Proceedings of: "The lithosphere in Italy". Acc. Naz. dei Lincei, vol. 80, pp. 41–61.
Niu, Y., Batiza, R., 1991a. DENSCAL: a program for calculating densities of silicate melts and mantle minerals as a function of pressure, temperature, and composition in melting range. Comput. Geosci. 17 (5), 679–687.
Niu, Y., Batiza, R., 1991b. In situ densities of silicate melts and mantle minerals as a function of temperature, pressure and compositions. J. Geol. 99, 767–775.
Niu, Y., Batiza, R., 1991c. An empirical method for calculating melt compositions produced beneath mid-ocean ridges: applications for axis and off axis (seamounts) melting. J. Geophys. Res. 96 (B13), 21753–21777.
Panza, G.F., Mueller, St., Calcagnile, G., 1980. The gross features of the lithosphere–asthenosphere system in Europe from seismic surface waves and body waves. Pageoph 118, 1209–1213.
Parsons, B., Sclater, J.G., 1977. An analysis of the variation of ocean flor bathymetry and heat flow with age. J. Geophys. Res. 82, 803–827.
Pasquale, V., Verdoya, M., Chiozzi, P., 1999. Thermal state and deep earthquakes in the Southern Tyrrhenian. Tectonophysics 306, 435–488.
Pasquale, V., Verdoya, M., Chiozzi, P., 2003. Heat-flux budget in the southeastern continental margin of the Tyrrhenian basin. Phys. Chem. Earth 28, 407–428.
Patacca, E., Sartori, R., Scandone, P., 1990. Tyrrhenian basin and Appenninic Arcs: kinematic relations since Late Tortonian times. Mem. Soc. Geol. Ital. 45, 453–462.
Pinna, E., Rapolla, A., 1979. Strutture crostali nell'Italia Meridionale da dati gravimetrici. Pubbl. n.235, Progetto Finalizzato Geodinamica, CNR.
Pontevivo, A., Panza, G.F., 2002. Group velocity tomography and regionalization in Italy and bordering areas. Phys. Earth Planet. Inter. 134, 1–15.
Recq, M., Rehault, J.P., Steinmetz, L., Fabbri, A., 1984. Amincissement de la croute et accretion au centre du Bassin Tyrrehenien d'apres la sismique refraction. Mar. Geol. 55, 411–428.
Rehault, J.P., Bethoux, N., 1984. Earthquake relocation in the Ligurian Sea (Western Mediterranean): geological interpretation. Mar. Geol. 55, 429–445.
Royden, L., Patacca, E., Scandone, P., 1987. Segmentation and configuration of subducted lithosphere in Italy: an important control on thrust-belt and foredip basin evolution. Geology 15, 714–717.
Sartori, R., 1989. Evoluzione neogenico-recente del bacino tirrenico e i suoi rapporti con la geologia delle aree circostanti. Gior. Geol. 3 (51/2), 1–39.
Scarascia, S., Lozej, A., Cassinis, R., 1994. Crustal structures of the Ligurian, Tyrrhenian and Ionian Seas and adjacent onshore areas

interpreted from wide-angle seismic profiles. Boll. Geofis. Teor. Appl. XXXVI (141-144), 5–19.

Schott, J., Schmeling, H., 1998. Delamination and detachment of a lithospheric root. Tectonophysics 296, 225–247.

Sebastian, A., 1989. NORMOD: a program for modal norm calculation and evaluation of other component transformations. Comput. Geosci. 15 (8), 1241–1248.

Selvaggi, G., 2001. Strain pattern of the southern Tyrrhenian slab from moment tensor and deep earthquakes: implications on the down-deep velocity. Ann. Geofis. 44 (1), 155–165.

Selvaggi, G., Chiarabba, C., 1995. Seismicity and P-wave velocity image of the Southern Tyrrhenian subduction zone. Geophys. J. Int. 121, 818–826.

Spadini, G., Cloetingh, S., Bertotti, G., 1995. Thermo-mechanical modeling of the Tyrrhenian Sea: lithospheric necking and kinematics of rifting. Tectonics 14, 629–644.

Spakman, W., Van der Lee, S., Van der Hilst, R., 1993. Travel-time tomography of the European–Mediterranean mantle down to 1400 km. Phys. Earth Planet. Inter. 79, 3–74.

Spear, F.S., Rumble III, D., Ferry, J.M., 1982. Linear algebraic manipulation of *n*-dimensional composition space. In: Ferry, J.M. (Ed.), Reviews in Mineralogy: Min. Soc. America, vol. 10, pp. 1–31. chapt. 1.

Spohn, T., Shubert, G., 1982. Convective thinning of the lithosphere: a mechanism for the initiation of continental rifting. J. Geophys. Res. 87, 4669–4681.

Steinmetz, L., Ferrucci, F., Hirn, A., Morelli, C., Nicolich, R., 1983. A 550 km long Moho traverse in the Tyrrhenian Dea from O.B.S. recorded Pn waves. Geophys. Res. Lett. 10, 428–431.

Suhadolc, P., Panza, G.F., 1989. Physical properties of the lithosphere–asthenosphere system in Europe from geophysical data. Proceedings of: "The lithosphere in Italy". Acc. Naz. dei Lincei, vol. 80, pp. 15–40.

Thisseau, C., Rehault, J.P., Foucher, J.P., 1986. Modèles thermiques et hypothèses sur la nature de la croute au centre de la Mer Tyrrhènienne. Mem. Soc. Geol. Ital. 36, 109–122.

Toksoz, M.N., Hsui, A.T., 1978. Numerical studies of back-arc convection and the formation of marginal basins. Tectonophysics 50, 177–196.

Turcotte, D.L., Subert, G., 1982. Geodynamics. Application of Continuum Physics to Geological Problems. John Wiley, New York.

Valera, J.L., Carminati, E., Negredo, A.M., Doglioni, C., 2003. Subcrustal seismicity in italy: control of rheology and phase changes. Geophys. Res. Abstr., 5.

Wang, C.Y., Awang, W.T., Yaolin, S., 1989. Thermal evolution of a rift basin: the Tyrrhenian Sea. J. Geophys. Res. 94 (B4), 3991–4006.

White, R., McKenzie, D., 1988. Magmatism at rift zones: the generation of volcanic continental margins and flood basalts. J. Geophys. Res. 94 (B6), 7685–7729.

Zito, G., Mongelli, F., de Lorenzo, S., Doglioni, C., 2003. Geodynamical interpretation of the heat flow in the Tyrrhenian Sea. Terra Nova 15, 425–432.